ELSEVIER

The potential of rapid cooling spark plasma sintering for metallic materials

Faming Zhang[1,*], Michael Reich[2], Olaf Kessler[2] and Eberhard Burkel[1]

[1] Chair of Physics of New Materials, Institute of Physics, University of Rostock, 18055 Rostock, Germany
[2] Chair of Materials Science, Faculty of Mechanical Engineering and Marine Technology, University of Rostock, 18059 Rostock, Germany

Spark plasma sintering (SPS) is a remarkable technique for consolidating a large variety of advanced materials with rapid heating rates. However, adjusting the cooling rates has so far faced limitations. This communication discusses the potentials of SPS integrated with a novel gas quenching system that can allow metallic materials to be sintered and rapidly quenched directly after the sintering step, saving energy and costs. Results on numerical simulations of rapid cooling-SPS and the mechanical properties and microstructures of Ti6Al4V alloy are discussed; exhibiting the feasibility of this *rapid cooling SPS* technique and the major implications for the field of SPS and metallic powder consolidation.

Introduction

Spark plasma sintering (SPS), commonly also defined as field assisted sintering (FAST) or pulsed electric current sintering (PECS) is a novel pressure assisted PECS process utilizing ON–OFF DC pulse energizing. With the repeated application of an ON–OFF DC pulse voltage and current in powdered materials, the spark discharge point and the Joule heating point (local high temperature-state) are transferred and dispersed over the overall specimen [1,2]. The main advantage of SPS over more conventional sintering techniques lies in its ability to rapidly sinter traditionally difficult-to-sinter materials to full density [3]. During SPS treatment, powders contained in a die can be processed for diverse new and traditional bulk material applications, for example, nanostructured materials [4,5], functional graded materials [6], hard alloys [7], titanium alloys [8], bioceramics [9], porous materials [10], diamonds etc. [11]. Some modifications to the SPS technique have been applied in recent years. Anselmi-Tamburini *et al.* [12] modified the SPS die materials and set-up to create high pressures of up to 1 GPa, by which fully stabilized zirconia and ceria ceramics with grain sizes approaching 10 nm could be obtained. Morsi *et al.* [13] modified SPS to a spark plasma extrusion process, whereby aluminum samples with extruded geometries could be prepared. SPS has very high heating rates of up to 1000°C/min, but its cooling rates are very slow with natural cooling or argon gas flooding. To date, the adjustment of cooling rates during SPS and the effects on the microstructures and properties of materials has been scarcely reported in the literature.

Sinter hardening is a hardening method used for powder metallurgy (PM) in which the parts are sintered and quenched directly after the sintering step, saving energy and costs connected to conventional hardening where the parts have to be reheated to hardening temperature [14–16]. Furthermore, sinter hardening is performed by gas quenching instead of oil quenching, creating benefits in terms of the dimensional stability and cleanliness of the specimen. Because of the poor thermal transfer characteristics (lower cooling rate) of gases under normal conditions, the gases must be optimized by proper adjustment of gas pressure and flow speed. In principle, gas quenching can be performed in two ways [17–20], namely: at low or atmosphere pressure with a high gas velocity; or at high pressure with limited gas velocities. In this short communication, the SPS technique was modified and integrated with a novel gas quenching system. The SPS vacuum was broken and flooded with argon gas and then quenched with high-velocity nitrogen gas. An $\alpha + \beta$ Ti6Al4V alloy was used as a model material. The heat transfer coefficient of the Ti6Al4V alloy during quenching was numerically simulated, and the effects of the cooling rate on the mechanical properties and microstructures of the alloy were investigated. The results prove the feasibility of the rapid cooling-SPS process and open the door for the processing of numerous other metallic powder-based material systems.

*Corresponding author:. Zhang, F. (faming.zhang@uni-rostock.de)

 1369-7021/06/$ - see front matter http://dx.doi.org/10.1016/j.mattod.2013.05.005

Methods and materials

Ti6Al4V powder with particle sizes of about 20 μm was obtained from TLS Technik GmbH & Co., Germany. The SPS experiments were conducted using a Model HP D-125 FCT SPS system (FCT System GmbH, Rauenstein, Germany) installed at the University of Rostock. Fig. 1(a), (b) shows the schematic diagram and image of the gas quenching system in the SPS. The system is rotationally symmetric, with six nozzles in one group and eight groups arranged around the sintered component. The gas is distributed evenly from all nozzles. The gas nozzle field is positioned inside the SPS chamber and quenches the sintered component together with the graphite tool directly after sintering without any movement of the component. The core temperature is measured by a central pyrometer with a focus point at the bottom of the central borehole of the graphite punch (labeled f). The Ti6Al4V powders were first pressed into an ∅40 mm graphite die, and sintered at 850°C and 50 MPa under vacuum. A heating rate of 100°C/min was applied, and the sintering process typically lasted 6 min. The applied direct current for the SPS process was 1000 A–2000 A with a pulse duration of 10 ms and an interval of 5 ms. During the cooling, the SPS furnace was flooded with argon gas to 4 kPa at rate of 10 l/min, maintaining the sintering temperature. It was then quenched from 850°C with room temperature nitrogen gas at a very high flow rate of 8000 l/min from the nozzles. Afterwards the nitrogen gas was released from the chamber to an internal gas pressure of 100 Pa–200 Pa. The various cooling rates were achieved by changing the thickness of the graphite dies. The sample dimensions measured 40 mm in diameter and 10 mm–12 mm in height.

The heat transfer coefficients are of interest for the characterization of the nozzle field's cooling effect. These are determined by means of cooling curve measurement and inverse thermal simulation by finite element (FE) software MSC.MARC 2010.1.0, and enable the thermophysical properties of the surrounding graphite die to be considered. In the calculation, the boundary conditions (and the heat transfer coefficients) of the FE-model are varied until the simulated and experimental temperature curves coincide. In the quenching experiments, the temperatures at four sites of the system are measured via pyrometer and thermocouples. As shown in Fig. 1(a), the center of the sample (A) is measured by the pyrometer; the surface of the sample (B) is measured by thermocouple T_1, the temperature in the middle of the graphite form (C) is measured by T_2 and the temperature of the lower graphite cone is measured by T_3. The numerical simulations used a rotation-symmetric finite-element-model considering the axial symmetry. After SPS the density of the sintered alloys was determined by the Archimedes method using water immersion. Then, the samples were machined into small cylinders measuring 8 mm in diameter and 10–12 mm in height. The hardness of the polished samples was measured with a SHIMADAZU Micro Hardness tester HMV at HV1. Their compressive strength and ductility were measured according to standard DIN 50106 on an Instron 8502 testing machine at room temperature with a compression speed of 0.5 mm/min. In the compressive tests, five samples for one group were tested to generate statistic results. The phase analysis of the Ti alloys was performed using diffraction experiments with high energy synchrotron radiation at Beamline P02.2 (DESY/PETRA) with a wavelength of 0.29118 Å (42.58 keV). The fracture surfaces of the compressed samples were analyzed using scanning electron microscopy (SEM, Zeiss Supra25) at 20 keV. The alloys were polished and etched by Weck's reagent for 20 s and subjected to optical microscopy to observe metallographic morphologies.

Results

Various cooling rates can be achieved by changing the thickness of the graphite forms. Fig. 2(a) shows the temperature–time cooling curves of the spark plasma sintered Ti6Al4V alloys with various cooling rates. Below 400°C, the pyrometer cannot measure the temperature of the sample. From the cooling curves, the average cooling rates of 1.6°C/s, 4.8°C/s, 5.6°C/s and 6.9°C/s with an uncertainty of 0.1°C/s were derived by taking the cooling time from 850°C to 400°C into account. The cooling rate of 1.6°C/s was achieved with a 20 mm thick graphite die with

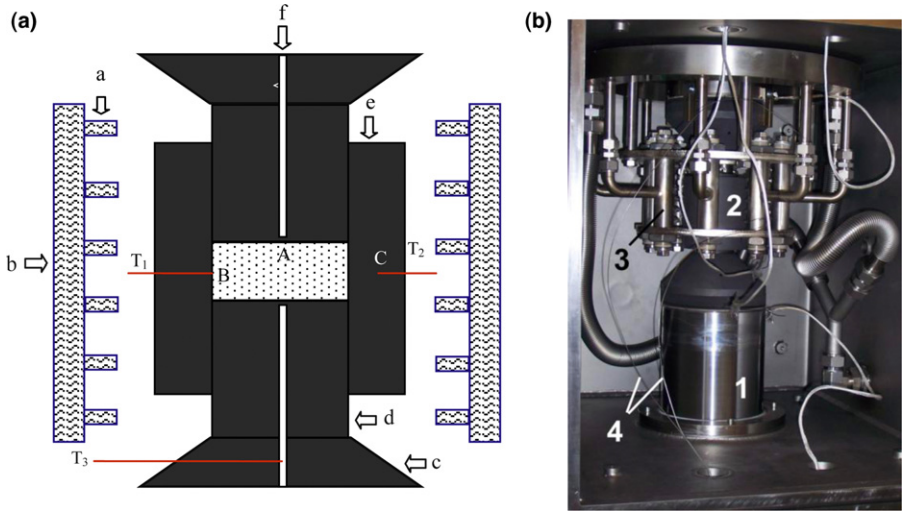

FIGURE 1

Schematic diagram (a) of the apparatus for spark plasma sintering with gas quenching system (a, gas nozzles; b, gas tube; c, graphite cone; d, graphite punch; e, graphite form; f, pyrometer hole for temperature measurement of the sample center A; T_1, T_2 and T_3, thermocouples for temperature measurement of the sample surface B, graphite form C, and graphite cone, respectively), and image (b) of SPS vacuum chamber (1, machine stamp, 2, sample block, 3, gas nozzle field, 4, thermocouples).

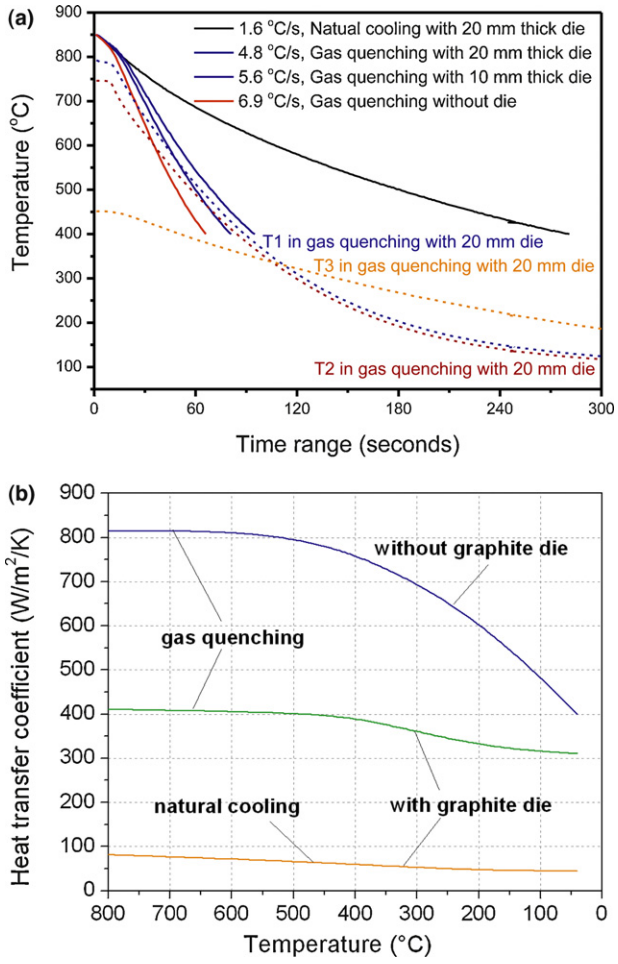

FIGURE 2

The cooling curves of the Ti6Al4V alloy as a function of time (a): (solid lines) pyrometer temperature values with various quenching rates and (dash lines) thermal couple values (T_1, T_2, T_3) in gas quenching with 20 mm thick die, and (b) the determined heat transfer coefficients of natural cooling (1.6°C/s) and gas quenching of the Ti6Al4V alloys with a 20 mm thick die (4.8°C/s) and without die (6.9°C/s).

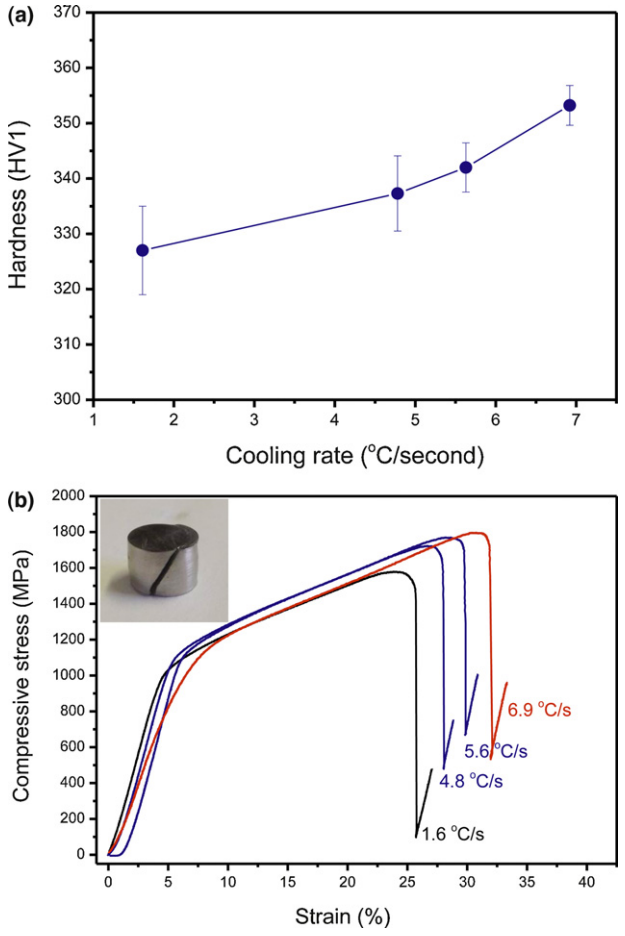

FIGURE 3

Hardness (HV1) (a) and compressive stress–strain curves (b) of the Ti6Al4V alloys at various cooling rates, exhibiting the improved hardness, ultimate compressive stress and ductility. Insert: image of a fractured specimen.

natural cooling, 4.8°C/s with a 20 mm die with gas quenching, and 5.6°C/s with a 10 mm die, also with gas quenching. The rate of 6.9°C/s was achieved in two steps: the powder sample was first sintered at 500°C for 5 min at 50 MPa in the die to get a 70–80% relative density, and then heated to a sintering temperature of 850°C to full densify it without the die, and the specimen was later directly gas quenched. Various cooling rates may be achieved in this way. The dashed lines show the temperature values from thermocouples during gas quenching with a 20 mm die. At the sintering temperature, the temperature of the graphite form (T_2) is lower than that of the sample surface (T_1) and T_1 is lower than the temperature in the center of the samples, as measured by the pyrometer. The temperature gradient exists during the sintering process as well as during the cooling process. The gas quenching starts from the outer surface of the graphite form: the temperature of the graphite cone (T_3) is reduced from 450°C to about 200°C after 300 s of gas quenching, but T_1 and T_2 decrease to below 80°C in this time. This indicates that gas quenching is only effective in cooling the graphite form and sample in the gas nozzle fields.

In addition to varying the cooling rate through the wall thickness of the dies, further variation of the cooling rate is possible by adjusting the gas flow rate and gas nozzle field geometry. Fig. 2(b) shows the numerically determined heat transfer coefficients of natural cooling and gas quenching of the Ti6Al4V samples. The heat transfer coefficients are reduced with decreasing temperatures for the samples processed with natural cooling (20 mm thick die) and gas quenching with (20 mm thick die) and without dies. From 800°C to 400°C, the coefficient values are higher than those below 400°C. This indicates that heat transfer and dissipation are faster at higher temperatures, above 400°C. The natural cooling sample exhibited a heat transfer coefficient of 80 W/(m^2 K) at 800°C which is gradually reduced to 50 W/(m^2 K) at room temperature. The gas quenched sample with a die exhibited a heat transfer coefficient of about 400 W/(m^2 K) at 800°C and dropped to about 300 W/(m^2 K) at room temperature. Quenching without a die results in a heat transfer coefficient of about 810 W/(m^2 K) at 800°C and 400 W/(m^2 K) at room temperature. The quenching intensity without a die is about two times higher than that with a die. However, the gas quenching with a die is also effective to increase the heat transfer coefficients up to five to seven times higher than natural cooling. The heat transfer coefficient is defined as the heat flux divided by the temperature difference.

The value of the heat transfer coefficient is proportional to that of the quenching intensity which can be described by the heat flux density on its surface. With higher heat transfer coefficients it can cool the sample faster, hence, the Ti alloys can be cooled rapidly with gas quenching due to the higher heat transfer coefficients. The sintering and quenching heat-treatment have been completed by one step SPS process without a separate heat treatment operation.

Fig. 3(a) shows the hardness (HV1) of the Ti6Al4V alloy with various cooling rates. All the Ti6Al4V alloys with various cooling rates have similar relative densities of above 99.0%. The naturally cooled samples with a cooling rate of 1.6°C/s have a hardness of 327 ± 8. The gas quenched samples exhibit a hardness of 337 ± 7, 342 ± 4 and 353 ± 4 for cooling rates of 4.8, 5.6 and 6.9°C/s, respectively. The hardness increases with a higher cooling rate, thus, sinter hardening of the Ti6Al4V alloys has been realized by SPS with gas quenching. Fig. 3(b) shows the compressive stress–strain curves of the Ti6Al4V alloys with various cooling rates. The stress–strain curves show the elastic deformation, plastic deformation and fracture stages. The insert image shows one of the fractured Ti6Al4V specimens. It is found that the fracture takes places at an angle of about 45° to the direction of the compressive load. The compressive yield strengths for all the samples are around 1100 MPa, which is higher than the reported values [21,22] (of about 902 MPa). But the ultimate compressive strength has increased with a higher cooling rate, as well as the compressive strains (ductility). Statistically, the samples with natural cooling rate of 1.6°C/s show the ultimate compressive strength of 1578 MPa ± 80 MPa and ductility of (26 ± 2)%. At a cooling rate of 4.8°C/s, they reach to (1723 ± 63) MPa and (28 ± 2)%, respectively. At a 5.6°C/s cooling rate, the strength is increased to (1775 ± 70) MPa and (30 ± 2)%; at 6.9°C/s this is raised to (1832 ± 43) MPa and (34.0 ± 3)%. The rapid cooling has increased the ultimate compressive strength and the ductility of the Ti6Al4V alloys.

Fig. 4(a) shows high energy X-ray diffraction patterns of the Ti6Al4V alloys. The raw Ti6Al4V powder shows the α-Ti phase. The naturally cooled sample show both the α and β-Ti phases and weak diffraction peaks from the α-Ti (1 1 2) and (2 0 1) lattice planes. The gas quenched Ti6Al4V alloys exhibit sharper diffraction peaks corresponding to Ti-rich phases with a β-Ti phase, as wells as new broad peaks probably from intermetallic phase of Al_2Ti (ICDD No.

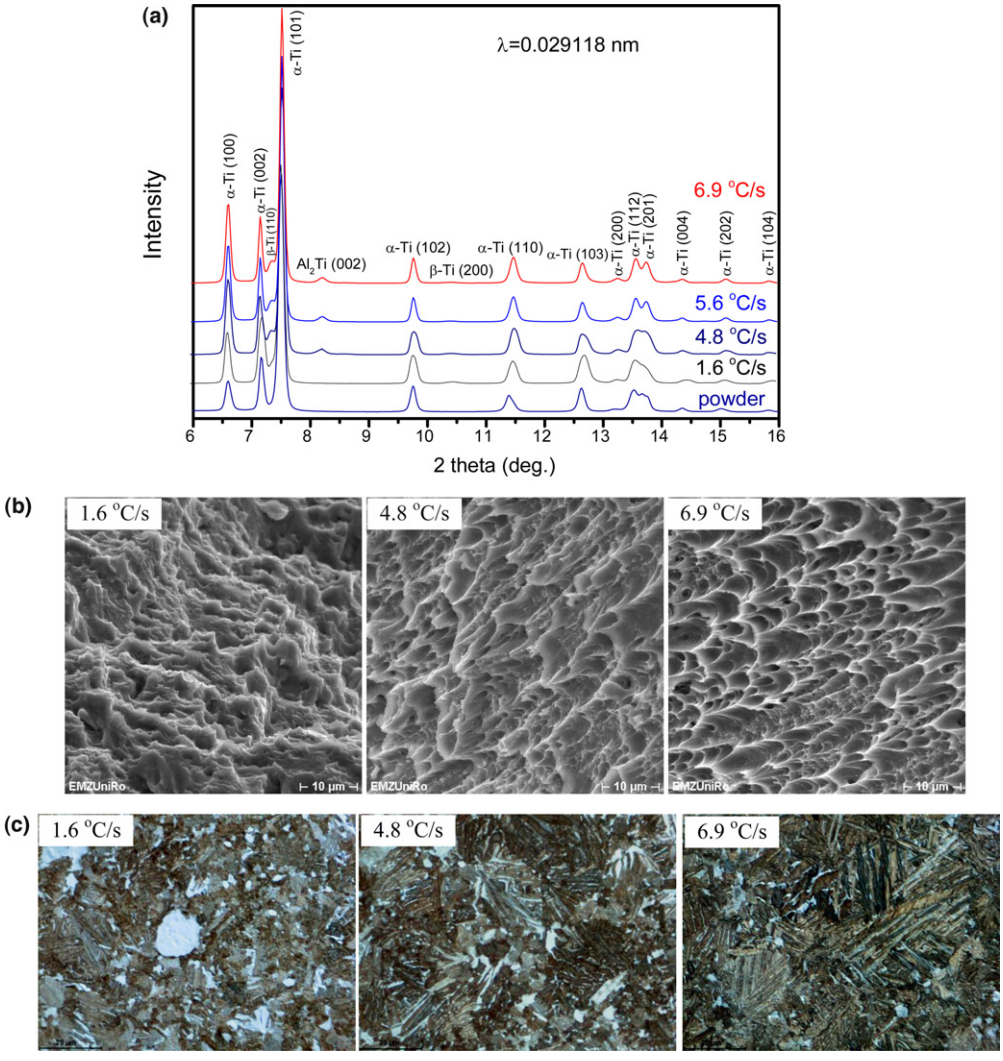

FIGURE 4

Synchrotron radiation high energy X-ray diffraction pattern (a), SEM micrographs of the fracture surfaces (b) and metallographic micrographs of the surfaces (c) of the Ti6Al4V alloys at various cooling rates of 1.6°C/s, 4.8°C/s, 6.9°C/s.

TABLE 1

Mechanical properties and phases of the Ti6Al4V alloys prepared by rapid cooling SPS at various cooling rates.

Cooling rate (°C/s)	Hardness (HV 1.0)	Ultimate compressive stress (MPa)	Ductility (%)	Phase compositions
1.6	327 ± 8	1578 ± 80	26 ± 2	α-Ti and β-Ti
4.8	337 ± 7	1723 ± 63	28 ± 2	α-Ti, β-Ti, Al_2Ti
5.6	342 ± 4	1775 ± 70	30 ± 2	α-Ti, β-Ti, Al_2Ti
6.9	353 ± 4	1832 ± 43	34 ± 3	α-Ti, β-Ti, Al_2Ti

42-1136). The gas quenching in the SPS resulted in the formation of nanocrystalline intermetallic phase of Al_2Ti in the alloys. Fig. 4(b) shows SEM micrographs of the fracture surface of the processed Ti6Al4V alloys. The samples all present a ductile fracture mode with a large amount of plastic deformation undergoing transgranular fracture with typical dimples. However, the fracture surfaces present more and more dimples with an increase of the cooling rate, indicating the sample becomes much more ductile after the rapid cooling in the SPS. Fig. 4(c) provides the metallographic morphology of the Ti6Al4V alloys with various cooling rates. In the etched metallographic images, the β-Ti phase (bcc) appears in white and the α-Ti phase (hcp) darker. The samples all show both phases in the microstructures. The naturally cooled sample with 1.6°C/s cooling rate shows a relative homogeneous globular α + β microstructure. The rapidly cooled sample shows a different microstructure with a lamellar α phase. As the cooling rate increases, the 6.9°C/s cooled sample has even more lamellar α phase. In general, gas quenching in the SPS results in a morphological change to the lamellar α-Ti phase.

Discussion

The hardness, ultimate compressive strength and ductility of the Ti6Al4V alloys have been increased due to the gas quenching. Sinter hardening is applicable for the Ti6Al4V alloy in which the samples are spark plasma sintered and gas quenched directly after the sintering. It saves energy and costs when compared with conventional hardening, in which the parts must be reheated to the hardening temperature. The microstructure analysis revealed that the rapid cooling led to the precipitation of intermetallic phase (Al_2Ti), more pronounced dimples in fracture surfaces, and a morphological change to lamellar α-Ti phase. Table 1 summarizes the mechanical properties and phases of the Ti6Al4V alloys prepared by rapid cooling SPS at various cooling rates. The hardness, ultimate compressive strength and ductility of the Ti6Al4V alloys were increased corresponding to the phase variations.

SPS is a nonequilibrium sintering process. Because of the higher cooling rates, the soluble Al, V elements in Ti have not enough time to diffuse, and then precipitate as second phases in the Ti6Al4V alloy. The precipitated nanocrystalline Al_2Ti can harden and dispersion reinforce the Ti6Al4V alloys, and therefore, the mechanical properties of the Ti6Al4V alloy are increased. Quenching from the α + β phase field can produce a microstructure that consists of a primary α phase, retained β-Ti, new α-Ti formed during quenching and intermetallic precipitates. With increasing cooling rates, the newly formed α-Ti becomes more lamellar. The lamellar structured α-Ti phase can lead to an increase in ductility of the Ti6Al4V alloy [23].

Using industrial gases for quenching of high value parts offers significant environmental and performance advantages over liquid quenching (water, oil, etc.). Gas quenched parts are clean, thus eliminating the need for post-cleaning operations. Because of the poor thermal transfer characteristics (lower cooling rate) of gases under normal conditions, they have to be optimized by proper adjustment of the gas pressure and flow speed. Gas quenching can be performed at low pressure with a high gas velocity or at high pressure with limited gas velocities [17–20]. In this study, we used the first method in the SPS, at low or atmospheric pressure with a high gas velocity. The flow rate of the nitrogen gas from the nozzles was 8000 l/min, and the pressure of gas was only slightly above normal atmospheric pressure. The thermo-physical properties of the gas are also an important issue. On the basis of availability, and the thermo-physical properties, hydrogen would appear to be good a choice as a quenching agent [24]; however, because of the explosive risks associated with hydrogen it is seldom used as a quench gas in commercial heat treating. Helium is almost as fast as hydrogen, not explosive, but significantly more expensive [25]. Nitrogen is the most popular choice, primarily because it is readily available and inexpensive [26], although argon is used in some special applications, but it does not quench as effectively as nitrogen and is considerably more expensive [27].

Summary

Ti6Al4V alloys have been used in medical applications for several decades, but one of the main problems of this alloy in biomedical applications is its insufficient ductility [28]. This investigation indicates that the traditional Ti6Al4V alloy can be modified by rapid cooling SPS leading to various mechanical changes. The high ductile Ti6Al4V alloy achieved through rapid cooling SPS offers unprecedented opportunities for the easy manufacturing of complex shapes and plates for biomedical and new engineering applications. Rapid cooling SPS combining sintering and gas quenching provides a novel method to tailor the mechanical properties of the Ti6Al4V alloys. It must be pointed out that this rapid cooling SPS is mainly suitable for metallic materials including metals, alloys and metal matrix composites. In general, ceramic materials will probably crack after quenching due to their poor thermal shock resistance. It is a subject of an ongoing investigation.

SPS integrated with gas quenching has been discussed for the first time for the successful modification of Ti6Al4V alloys. Cooling curve measurements and inverse thermal FE simulations reveal that the gas quenching can increase the heat transfer coefficient up to five to seven times. The cooling rates ranging from 1.6°C/s to

6.9°C/s were achieved by changing the thickness of the graphite dies. Sinter-hardening of the Ti6Al4V alloy has been achieved, where the hardness rises from 327 to 353 HV1. The gas quenching has increased the ultimate compressive strength and ductility of the Ti6Al4V alloy from 1578 MPa to 1832 MPa and from 26% to 34%, respectively. The microstructure analysis revealed that the rapid cooling led to the precipitation of nanocrystalline intermetallic phase (Al_2Ti), more pronounced dimples in fracture surfaces and a morphological change to lamellar α-Ti phase.

Rapid cooling SPS can be applied to a wide range of metals, alloys and metal matrix composites, where the parts can be rapidly sintered and rapidly quenched directly after the sintering step, saving energy and cost. Future work will involve adjusting gas flow rate and gas nozzle field geometry, and examine the effects of cooling rates on keeping grain sizes of nanocrystalline metallic materials.

Acknowledgement

This work was gratefully supported by the DFG GRK1505/1 (Welisa). The technical assistance from Mr. Y. Quan is acknowledged. The authors also thank Dr. H.P. Liermann for his supports at the beamline P02.2.

References

[1] Z.A. Munir, et al. J. Mater. Sci. 41 (2006) 763.
[2] Z.A. Munir, et al. J. Am. Ceram. Soc. 94 (2011) 1.
[3] M. Nygren, Z. Shen, Key Eng. Mater. 264–268 (2004) 719.
[4] M. Nygren, Z. Shen, Solid State Sci. 5 (2003) 125.
[5] R. Sivakumar, et al. Scripta Mater. 56 (2007) 265.
[6] F. Watari, et al. Compos. Sci. Technol. 64 (2004) 893.
[7] F. Zhang, et al. J. Alloys Compd. 385 (2004) 96.
[8] F. Zhang, et al. J. Biomed. Mater. Res. B 94B (2010) 406.
[9] Y.W. Gu, et al. Biomaterials 25 (2004) 4127.
[10] F. Zhang, et al. Adv. Eng. Mater. 12 (2010) 863.
[11] F. Zhang, et al. Diamond Relat. Mater. 20 (2011) 853.
[12] U. Anselmi-Tamburini, et al. Scripta Mater. 54 (2006) 823.
[13] K. Morsi, et al. Scripta Mater. 61 (2009) 395.
[14] M. Dlapka, et al. J. Heat Treat. Mater. 67 (2012) 223.
[15] S.N. Thakuc, et al. Int. J. Powder Metall. 40 (2004) 45.
[16] L.A. Dobrzanski, M. Musztyfaga, J. Achiev. Mater. Manuf. Eng. 37 (2009) 630.
[17] N. Lior, J. Mater. Process. Technol. 1881 (2004) 155.
[18] M. Reich, et al. Key Eng. Mater. 424 (2010) 57.
[19] S. Schöne, et al. Proc. 3rd International Conference on Distortion Engineering 2011, September 14–16, Bremen, Germany, (2011), p. 75.
[20] M. Reich, O. Kessler, in: D. Scott MacKenzie (Ed.), Proc. 6th Int. Quenching and Control of Distortion Conf., 9–13 September 2012, Chicago, IL, USA, ASM International, 2012, p. 563.
[21] M. Bram, et al. Met. Powder Rep. 61 (2006) 20.
[22] M.H. Lee, et al. J. Phys. D: Appl. Phys. 41 (2008) 105404.
[23] J.H. Kim, et al. Acta Mater. 51 (2003) 5613.
[24] B. Xiao, et al. J. ASTM Int. 8 (2011) 103403.
[25] J.H. Sung, et al. Solid State Phenom. 118 (2006) 221.
[26] H. Morii, et al. Nucl. Instrum. Methods Phys. Res. A 526 (2004) 399.
[27] C. McGee, et al. Surface Engineering Coatings and Heat Treatments 2002: Proceedings of the 1st ASM International Surface Engineering and the 13th IFHTSE Congress, ASM International, 2003 , p. 457.
[28] K.H. Frosch, K.M. Stürmer, Eur. J. Trauma 32 (2006) 149.